Engineering Structures 318 (2024) 118656

Contents lists available at ScienceDirect

Engineering Structures

journal homepage: www.elsevier.com/locate/engstruct

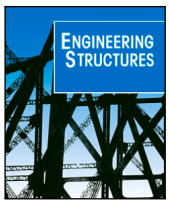

Semi-probabilistic calibration of material partial safety factors for the capacity assessment of existing masonry structures

Federica Vadalà [a,*], Luis C.M. da Silva [b], Ivo Caliò [c], Paulo B. Lourenço [a]

[a] Department of Civil Engineering, University of Minho, Institute for Sustainability and Innovation in Structural Engineering (ISISE), Guimarães, Portugal
[b] Department of Architecture, Built Environment and Construction Engineering (ABC), Politecnico di Milano, Milan, Italy
[c] Department of Civil Engineering and Architecture (DICAR), University of Catania, Catania, Italy

ARTICLE INFO

Keywords:
Sensitivity analysis
Partial safety factor
Existing masonry structures
Nonlinear static analysis

ABSTRACT

A practical procedure is presented for the calibration of partial safety factors (PSF) related to material properties, with a focus on unreinforced masonry structures. The methodology addresses the propagation of material and model uncertainties through a calibration based on the First Order Reliability Method (FORM) in the context of nonlinear static analysis approaches. The so-called Star Design with Central Point (SDCP) method is adopted for the computation of sensitivity coefficients and corresponding PSF for material uncertainty (γ_m). First, it is demonstrated how such calibration is affected by the geometry of the structure, by the pre-compression load level, and by the dominant failure mode. Second, it is evidenced that the most influential parameters on the structural response vary depending on the adopted modelling strategy (macro- or micro-modelling) for masonry discretisation. Third, the relative importance of model uncertainties is evidenced, for which a dataset of numerical predictions for the in-plane capacity of masonry panels is collected from the literature and discussed. Lastly, a comparison of different strategies to propagate uncertainty is provided, which emphasises the promising potential of the proposed procedure.

1. Introduction

The modelling of the seismic response of masonry structures is currently one of the most critical areas of research in both civil and conservation engineering due to their high vulnerability to earthquakes. Within a mechanical standpoint, masonry is generally represented through two modelling strategies: a macro-approach, where the material is smeared out and represented through an equivalent and homogeneous media, and a micro-approach, where the masonry components are explicitly modelled. In such a context, for each of the latter modelling approaches, numerical models based on the finite-element method (FEM) [1–5], discrete-element method (DEM) [6–10], discrete macro-element method (DMEM) [11–13], and discrete rigid body spring models (RBSM) [14–16] can be adopted. A comprehensive review of the existing modelling strategies for masonry structures is given in D'Altri et al.[17]. However, the prediction of the mechanical response of a masonry structure is complex. This is in part due to the combined effects of the aleatoric and epistemic uncertainties involved. While the former are generally associated with the inherent randomness of the geometric and material properties, the latter may arise from limited knowledge of the structural model parameters, as well as from the inherent limitations of available analytical and numerical strategies and the methods of analysis that can be adopted according to the code recommendations. Within this framework, a sound identification and propagation of uncertainty in the different steps involving the capacity assessment of existing masonry structures becomes essential to prevent severe structural failures and expensive repair costs. A full probabilistic approach represents the most rigorous strategy for addressing all the complex issues involved. Despite its increasing adoption at both the research level [18–21] and in recommendation documents, such as SAC-FEMA [22,23] and CNR-DT 212/2013 [24] guidelines, the implementation of this approach in engineering practice-oriented procedures continues to face challenges, primarily arising from the significant computational effort and expertise required for its application. To ensure practicability, the strategy generally employed in current standards, such as EN 1998-3 [25] and the Italian Structural Code [26], involves a semi-probabilistic approach based on the use of confidence factors (CF). For this purpose, a knowledge level (KL) is defined based on the quantity and quality of the information gathered through tests and inspections, which corresponds to a predefined value of the CF. Several studies [27–31] pointed out the limitations associated with this approach. The critical issues involve: (i) neglecting the dependence of the CF, besides the knowledge level, on other aspects such as the

* Corresponding author.
E-mail address: federica.vadala@civil.uminho.pt (F. Vadalà).

https://doi.org/10.1016/j.engstruct.2024.118656
Received 28 March 2024; Received in revised form 16 June 2024; Accepted 17 July 2024
Available online 31 July 2024

relative characteristics of the materials, the type and complexity of the structure, and the actual variability of the parameters influencing the structural response; (ii) the a-priori definition of the parameters that are affected by the CF; (iii) the use of a singular safety factor to account for the impact of various sources of uncertainties, without an explicit investigation of their effect on the safety assessment. However, only a few studies have proposed alternative strategies to address such limitations. Within this context, Franchin and Pagnoni [30] introduce a new perspective for the calibration of resistance-side safety factors (γ_{Rd}) compatible with the general Eurocode safety format. Specifically, their proposal aims at a more general definition for the γ_{Rd} in the computation of the design resistance R_d value, as outlined in EN 1990:2023 [32], as it tries to account for uncertainties associated with the resistance model and geometric deviations, as traditionally addressed, but also for uncertainties pertaining to material properties and construction details. The study focuses on a local (element-level) verification of a reinforced concrete structure, demonstrating the capability of the proposed format in providing tabulated values of γ_{Rd} for each resistance model proposed in the code [25]. Another strategy is proposed by Cattari et al. [29], in which a sensitivity analysis is introduced as an effective tool to support the seismic assessment across multiple aspects, such as the identification of the parameters that significantly influence the structural response, the optimisation of investigation and testing plans, the selection of the parameters to which apply a CF, along with the computation of CF values. In Haddad et al. [31], the potential of the use of sensitivity analysis is further explored through its introduction on the computation of two essential parameters (the median value of the Intensity Measure compatible with the attainment of a given Limit State, IM_{LS}, and the corresponding dispersion, β_{LS}) for the derivation of fragility curves. The CF is then computed by rearranging the closed-form expression proposed in Cornell et al. [23] for the calculation of the annual probability of occurrence. The study demonstrates the effectiveness of coupling the sensitivity analysis with the Star Design with Central Point (SDCP) method, yielding results comparable to those obtained through a more rigorous probabilistic approach while requiring a limited number of analyses.

In such a context, the present study proposes a practical procedure for the calibration of material partial safety factors (PSF), with a focus on unreinforced masonry structures. The propagation of both material and model uncertainty is accounted for through a calibration based on the First Order Reliability Method (FORM). In the former case, the approach introduces the use of sensitivity analysis combined with the SDCP method to compute the PSF for material uncertainty (γ_m), aiming to address the aforementioned shortcomings in the application of code-recommended CF. A calibration example is performed by accounting for different geometries, failure modes, and scales of analysis, i.e. at the scale of a panel and façade wall. Since the most influential parameters on the structural response may vary according to the adopted modelling strategy, the calibration is also processed considering a discrete approach and a FE-based continuum approach through both macro- and micro-modelling strategies. At last, it is noteworthy to stress that we also seek to represent model uncertainties in the estimation of the PSF, for which statistical parameters derived from a literature dataset of numerical predictions for shear–compression tests are considered.

The paper is organised as follows: Section 2 discusses the FORM-based calibration of partial safety factors adopted in this study; Section 3 delves into the numerical modelling strategies adopted; Section 4 details the calibration of partial safety factors considering material uncertainty (γ_m) at both panel and wall scale; Section 5 covers the calibration of partial safety factors (PSF) accounting for model uncertainty (γ_{Rd}); Section 6 explores the effects of employing different strategies to propagate uncertainty on the assessment of structural capacity in masonry structures; Section 7 reports the main findings and final remarks.

2. FORM-based calibration of partial safety factors

The calibration of partial safety factors for material properties is performed based on the First Order Reliability Method (FORM) [33] in accordance with EN 1990:2023 [32]. The latter defines the design resistance value R_d as:

$$R_d = \frac{1}{\gamma_{Rd}} \cdot R\left\{ \eta_i \cdot \frac{X_{k,i}}{\gamma_{m,i}}; a_d; \Sigma F_{Ed} \right\} \qquad i \geq 1 \tag{1}$$

Here, γ_{Rd} is the partial safety factor that accounts for (i) the uncertainty related to the resistance model, which can include simplified relationships or complex numerical models; and (ii) the potential geometric deviations if disregarded in the geometric modelling. The other quantities in Eq. (1) are the conversion factor η that accounts for the moisture, temperature, scale, and ageing effects (assumed here as $\eta = 1.0$, i.e. no effect); the characteristic value of the i-th material property X_k, which is affected by the partial safety factor γ_m to include material variability; the design values of geometrical properties a_d; and the design values for actions F_{Ed} used in the structural assessment. The last term is introduced to account for the dependence of the design resistance on actions, as for instance the case of resistance due to friction. For simplicity, the partial safety factors γ_m and γ_{Rd} may be combined into a single PSF for the material property ($\gamma_M = \gamma_m \gamma_{Rd}$), leading to the following expression:

$$R_d = R\left\{ \eta_i \cdot \frac{X_{k,i}}{\gamma_{M,i}}; a_d; \Sigma F_{Ed} \right\} \qquad i \geq 1 \tag{2}$$

The design value of a material property X can be expressed as $X_d = X_k/\gamma_m$. Consequently, a general expression for γ_m can be derived based on FORM as follows:

$$\gamma_m = \frac{X_k}{X_d} = \frac{F_x^{-1}(p)}{F_x^{-1}(\Phi(-\alpha \cdot \beta))} \tag{3}$$

in which F_x is the cumulative probability distribution function describing X, p is the fractile adopted to compute the characteristic value of X, Φ is the standard Normal cumulative distribution, α is the FORM sensitivity factor, and β is the reliability index. It has been evidenced by Jacinto et al. [34] that the probabilistic model adopted for a resistance variable has a significant impact on the partial factors calibration. To address such a concern [35–39], the material properties are herein modelled according to the Normal (ND), Lognormal (LND), and Weibull (WD) distributions. The general form of Eq. (3) can be adapted into three specific expressions, namely Eq. (4) for the Normal distribution, Eq. (5) for the Lognormal distribution, and Eq. (6) for the Weibull distribution (being k a shape parameter directly related to the coefficient of variation of X, i.e. V_x).

$$\gamma_m = \frac{1 + \Phi^{-1}(p) \cdot V_X}{1 - \alpha \cdot \beta \cdot V_X} \tag{4}$$

$$\gamma_m = exp\left(\sqrt{ln(1 + V_X^2) \cdot (\alpha \cdot \beta + \Phi^{-1}(p))} \right) \tag{5}$$

$$\gamma_m = \left(\frac{ln(1-p)}{ln(1 - \Phi(-\alpha \cdot \beta))} \right)^{\frac{1}{k}} \tag{6}$$

In general, the uncertainties in the resistance model are assumed to follow a lognormal distribution [34,40,41] and, therefore, the partial safety factor γ_{Rd} can be computed according to Eq. (7):

$$\gamma_{Rd} = \frac{1}{\theta_R} = \frac{1}{F_\theta^{-1}(\Phi(-\alpha_\theta \cdot \beta))} = \frac{1}{exp(m_\theta - \alpha_\theta \cdot \beta \cdot s_\theta)} \tag{7}$$

where θ_R is a random variable that describes the accuracy of the resistance model, F_θ is the cumulative probability distribution function describing θ_R, α_θ is the FORM sensitivity factor of θ_R, and m_θ and s_θ represent the sample mean and the sample standard deviation of the logarithm of θ_R, respectively. A key aspect of a FORM-based calibration of partial safety factors lies in the adoption of proper values for the sensitivity factors. The sensitivity α-value for a basic variable X describes

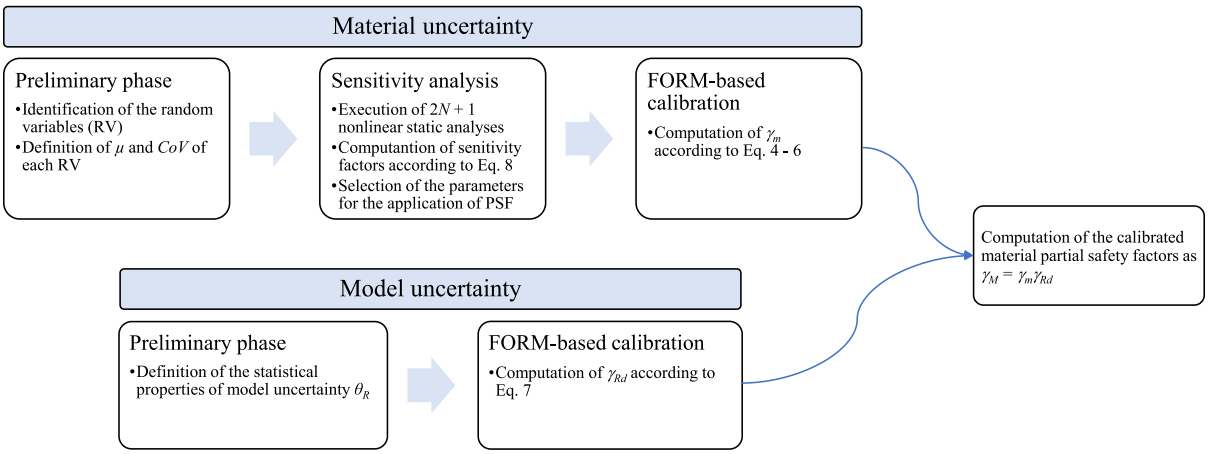

Fig. 1. Summary of the main steps for the proposed procedure for the calibration of material partial safety factors.

the effect of its variation on the attainment of the considered limit state. Both ISO 2394 [42] and EN 1990:2023 [32] propose constant values for the FORM sensitivity factors. Specifically, a value of 0.80 is suggested for dominating resistance parameters and 0.32 for the remaining parameters, provided that $0.16 < \sigma_S/\sigma_R < 7.6$, where σ_S and σ_R are the standard deviations of the dominating load and resistance parameters, respectively. When this condition is violated, an α-value of 1.0 should be adopted for the variables with the largest standard deviation and a value of 0.4 should be adopted for the remaining ones. Although the latter approach is generally conservative [43], it may ignore the relative characteristics of the materials, the structural type, the predominant failure mode, among other particular features of a structural system. A reliability-based code calibration analysis may overcome the latter, but it requires the explicit definition of a limit state function, which is generally unattainable in most nonlinear analysis within a multi degree of freedom system. Furthermore, this approach lacks practical applicability since it is based on a full probabilistic analysis. In such a context, a procedure is presented for the calibration of partial safety factors for material properties that still explores the concept of sensitivity factors. The proposed strategy allows to: (i) identify the material parameters that affect most the structural response; and (ii) calibrate partial safety factors that account for the actual sensitivity of the seismic response to each material parameter. Sensitivity factors are estimated through a sampling-based approach by computing the first-order Sobol' indices [44]. The Star Design with Central Point (SDCP) method is adopted as it allows to derive the actual sensitivity of the seismic response to each material parameter with a limited number of analyses [31], differently from a full probabilistic-based calibration [23,24]. The method consists in performing a set of $2N + 1$ nonlinear static analyses, being N the number of mechanical parameters assumed to be random variables (RV), in which: (i) a total of $2N$ numerical analyses are performed by considering both the lower and upper bounds of each random variable, and (ii) a single analysis, which serves as a reference, is conducted by considering the median values for the RV. A preliminary definition of the discrete values that characterise the interval range of a variable needs to be initially conducted. Specifically, three values designated as lower, upper, and median are attributed to each RV. The variations recommended by the updated version of EN 1998-3 [25] (under review) and the commentary document to the Italian Structural Code [26], as well as the information available in the literature or experimental tests on similar masonry typologies, can be considered as a reference. The sensitivity of the structural response to each i-th random parameter is evaluated by deriving the relative first order Sobol' index S_i according to Eq. (8), which reads as:

$$S_i = \frac{D_{V,i}}{D_V} = \alpha_i^2 \qquad i = 1, 2, \dots, N \tag{8}$$

where, D_V is the total variance associated with the model output and $D_{V,i}$ is the partial variance related to the i-th parameter. Based on the S_i values, the FORM sensitivity coefficients are derived since first-order Sobol' indices represent the squared α-factors [45]. Here, the partial variance $D_{V,i}$ is computed from the output of $2N + 1$ nonlinear static analyses as follows:

$$D_{V,i} = \frac{\sum_j (O_j - \overline{O})^2}{n - 1} \qquad j = 1, 2, \dots, n \tag{9}$$

where O_j is the output control parameter that is assumed to be the ultimate load derived from $n = 3$ numerical analyses, according to the lower, upper, and median values of the i-th parameter; $\overline{O}$ is the mean value of the three outputs for each i-th random variable.

The value of S_i ranges between $0.0 - 1.0$ and a higher value indicates that the variation of the corresponding parameter significantly influences the variation of the output control parameter. Thus, the calculation of sensitivity coefficients can provide insights into the key parameters that influence the structural response, which can be selected for the application of the PSF. Under this scope, a specific α-value (α_1) can be defined based on Eq. (9). This represents the minimum value below which the sensitivity of a material property can be disregarded as it would lead to a PSF value lower than one. The analytical expression of α_1 is determined by requiring that the PSF equals one in Eq. (3)-(5), which results in Eq. (10) regardless of the selected probabilistic distribution.

$$\alpha_1 = \frac{-\Phi^{-1}(p)}{\beta} \tag{10}$$

According to ISO 2394 [42] and EN 1990:2023 [32] guidelines, this study assigns the 5% fractile to the variable material parameters. Target values for the reliability index β of new structures are provided in the EN 1990:2023 [32], being a function of both the reference period and the consequence class (CC) of the building, i.e. based on the expected consequences of failure and the marginal cost of safety. A reduction in the target reliability index for existing structures has been acknowledged to be acceptable due to the higher marginal cost of safety [46,47]. In this regard, and following the recommendation provided by the Dutch standard [48], the reliability index for existing structures is reduced to 1.8, 2.5, and 3.3 for low, moderate, and high consequences of failure, respectively. As a result, the α_1-values are determined to be 0.90, 0.65, and 0.50, each corresponding to β values of 1.8, 2.5, and 3.3, respectively. The proposed procedure is implemented in the following sections according to the steps summarised in Fig. 1.

3. Numerical modelling approaches

The modelling of the adopted masonry prototypes is achieved through different strategies, including: (i) finite element (FE) macro-

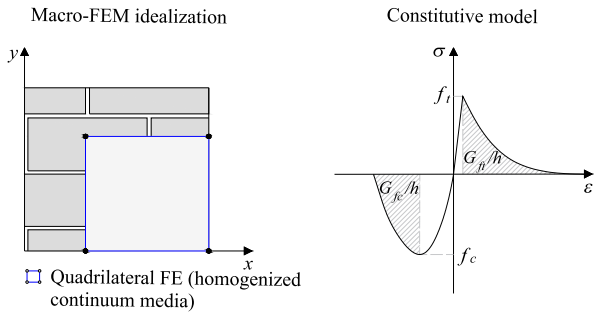

a) macro-FEM

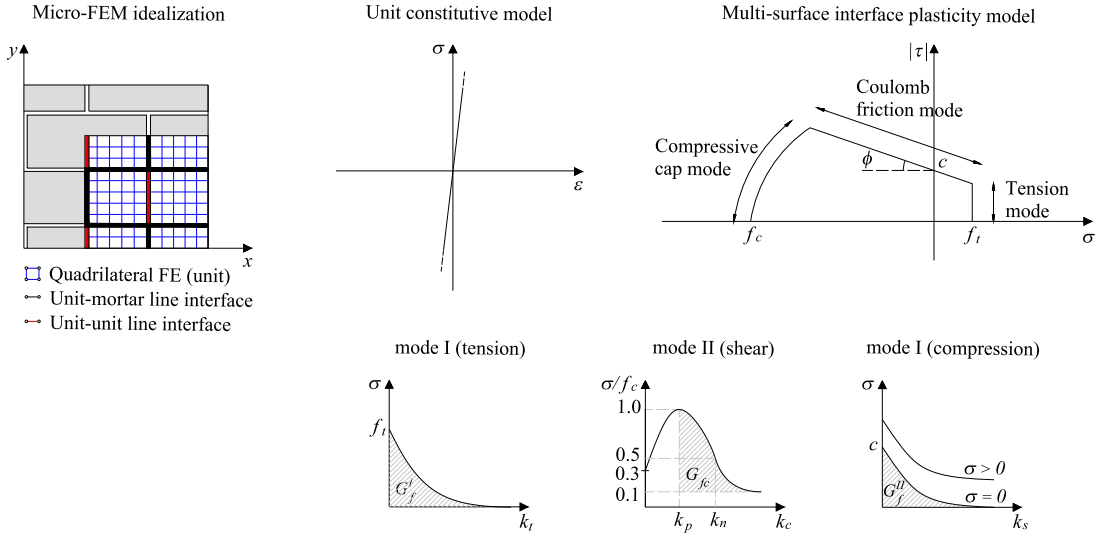

b) micro-FEM

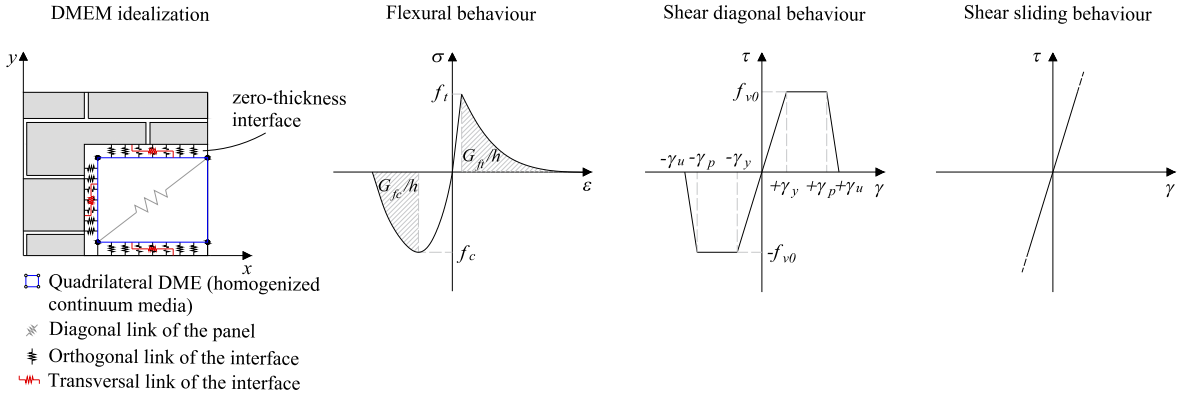

c) DMEM

Fig. 2. Constitutive models assumed in the modelling of the masonry prototypes. (For interpretation of the references to colour in this figure legend, the reader is referred to the web version of this article.)

model and a simplified micro-model approach by means of the FE software DIANA FEA [49]; and (ii) a macro-modelling approach using the discrete macro-element (DME) software HiStrA [50] (see Fig. 2). In the former case, masonry is modelled as a homogeneous isotropic continuum material through the Total Strain Rotating Crack Model (TSRM), which is based on a smeared cracking approach [51]. Exponential and parabolic softening are assumed in tension and compression, respectively. The macro-FE models are developed by adopting plane stress 8-node quadrilateral elements with a quadratic interpolation scheme (Q16M), in which the average mesh size is set equal to the 10% of the minimum dimensions of the panel geometries (i.e. 0.10 m), as proposed in Parisse et al. [52]. In the simplified micro-FE models, each unit is modelled through plane-stress quadrilateral elements (Q16M). The Mortar joints and potential brick cracks interfaces are modelled with

Table 1
Mechanical parameters assumed in the macro-models for the homogenised continuum media.

Model		ρ [kg/m^3]	ν [–]	E [N/mm^2]	f_t [N/mm^2]	G_{ft} [N/mm]	f_c [N/mm^2]	G_{fc} [N/mm]	f_{v0} [N/mm^2]	γ_p [–]	γ_u [–]
Macro-FEM	μ	1800	0.25	1850	0.25	0.01	6.2[1]	10.0	–	–	–
	CoV	–	–	20%[2]	21%[2]	20%	12.2%[1]	20%	–	–	–
DMEM	μ	1800	0.25	1850	0.25	0.01	6.2[1]	10.0	0.23	0.005	0.03
	CoV	–	–	20%[2]	21%[2]	20%	12.2%[1]	20%	21%[2]	20%	20%

Reference: 1 = experimental data [57,58]; 2 = updated version of EN 1998-3 [25].

Table 2
Mechanical parameters adopted in the simplified micro-FE models for the zero-thickness interface elements.

Interface		k_n [N/mm^3]	k_s [N/mm^3]	f_t [N/mm^2]	G_f^I [N/mm]	c [N/mm^2]	ϕ [–]	ψ [–]	G_f^{II} [N/mm]	f_c [N/mm^2]	G_{fc} [N/mm]
Mortar joints	μ	74.2	30.6	0.04[1]	0.001	0.23[1]	0.53[1]	0.349	0.02	6.2[1]	10.0
	CoV	20%	20%	25.7%[1]	20%	17.9%[1]	19%[3]	–	20%	12.2%[1]	20%
Potential brick cracks	μ	300	125	2.44[1]	0.1	2.0	0.60	0.349	0.1	26.9[1]	20.0
	CoV	20%	20%	25.8%[1]	20%	20%	20%	–	20%	9%[1]	20%

Reference: 1 = experimental data [57,58]; 2 = updated version of EN 1998-3 [25]; 3 = Probabilistic Model Code [40].

3+3 nodes interface elements (CL6CT). A linear elastic behaviour is assumed for the masonry units and material nonlinearity is lumped in the interfaces, to which the so-called combined cracking-shearing-crushing model is assigned. This model is based on a Mohr–Coulomb type friction surface combined with a tension cut-off and a compression cap [53,54]. The average size of the finite element mesh considered for the masonry units and their interfaces is set as equivalent to 0.03 m. Concerning the discrete (DME) discretisation strategy, masonry walls are modelled as an assemblage of three-dimensional (3D) quadrilateral macro-elements with rigid plane edges and hinged vertices. In-plane shear deformation is accounted through diagonal nonlinear links that connect two vertices of the quadrilateral element. The interaction of the macro-elements is governed by a discrete distribution of nonlinear links at the plane interfaces, which are responsible for simulating the flexural and sliding behaviour between panels, both in the in-plane and out-of-plane directions [55]. The DMEM approach requires the definition of the material parameters considering the flexural, shear-diagonal, and shear-sliding failure modes decoupled. To be consistent with the FE modelling strategies, the flexural response is modelled considering that the tensile and compressive post-peak behaviours are simulated by an exponential and a parabolic curve, respectively. The shear-diagonal behaviour is modelled by means of an elasto-plastic constitutive law with linear softening governed by a Turnšek-Cačovic yielding surface [56], whereas the sliding mechanism is considered inhibited. An average mesh size of 1.0 m is adopted for the DME models since it allows a reasonable compromise between computational effort and accuracy of results.

4. Material uncertainty

Partial safety factors (PSF) that account for material uncertainty γ_m are calibrated through the FORM-based strategy described in Section 2. First, such calculation is conducted at a panel scale for which two masonry panels with different in-plane aspect-ratios serve as benchmarks. In this regard, and prior to the calibration of the safety factors, the accuracy of the numerical models is assessed by comparing the results with the literature experimental data [57] (Section 4.1). With such a baseline, in Section 4.2 the calibration of the PSF is performed as a function of the geometry and failure mode captured for each panel and provided for the three modelling strategies adopted (Section 3). Afterwards, the numerical application at the wall scale is presented in Section 4.3.

4.1. Panel scale: numerical calibration

The in-plane cyclic shear tests conducted by Anthoine et al. [57] are selected as references. The experimental tests were conducted on two clay brick masonry walls, built with clay brick units of 250 × 120 × 55 mm^3 and 10 mm thick mortar joints and following an English bond pattern. The masonry panels were restrained according to a double-fixed boundary condition, but the top edge was free to move vertically so that the pre-compression level of $\sigma_0 = 0.6$ MPa remained constant throughout the experiment. Both panels have a base $B = 1.0$ m and thickness $t = 0.25$ m but different heights, i.e. a slender panel with $H = 2.0$ m and a squat panel with $H = 1.35$ m. Such geometries were chosen [57,58] in order to capture different failure mechanisms. The slender panel exhibited an in-plane flexural failure, while the squat panel attained a diagonal shear failure. The in-plane tests are simulated by means of a monotonic static nonlinear analysis and considering micro- and macro-modelling strategies (Section 3). The assumed material properties for the masonry components are given in Tables 1–3 according to each modelling strategy. The selected mean (μ) values and the coefficients of variation (CoV) follow the experimental data assumed as Ref. [57,58]. When applicable, the recommendations from the Probabilistic Model Code [40] and the updated version of EN 1998-3 [25] for solid clay brick masonry and lime mortar are also considered. The masonry density ρ, the Poisson's coefficient ν, and the dilatancy angles ψ are assumed to be deterministic variables. It is worth of noting that the FEM-based and DMEM-based models rely on different formulation that influence the key parameters governing the mechanical response. Several studies demonstrated the latter by conducting a calibration step in masonry panels based on the dominant failure mechanism et al. [59]. Therefore, although the tensile strength has similar values for both numerical strategies, these values have been objectively found according to a calibration that aimed to reproduce a similar response for the masonry panels.

Table 3
Mechanical parameters assumed in the simplified micro-FE models for the clay bricks.

	ρ [kg/m^3]	ν [–]	E [N/mm^2]
μ	1800	0.15	3000
CoV	–	–	20%

The consistency of the numerical models is assessed by comparing the experimental results [57] with the obtained load–displacement curves. Fig. 3 highlights that the experimental behaviour and collapse load are well reproduced by the numerical models for both masonry panels. The numerical crack pattern is provided in Fig. 4 and Fig. 5 at the peak load instant for the slender and the squat panels, respectively. In particular, the comparison is provided in terms of the maximum principal strain ($E_1 = \epsilon_{11}$) distribution for the macro-FE models, of relative displacement at the interface (DUX) for the simplified micro-FE models, and of the damage obtained by tensile or compression (in red) at the interfaces (in green) for the DME models. Furthermore, in

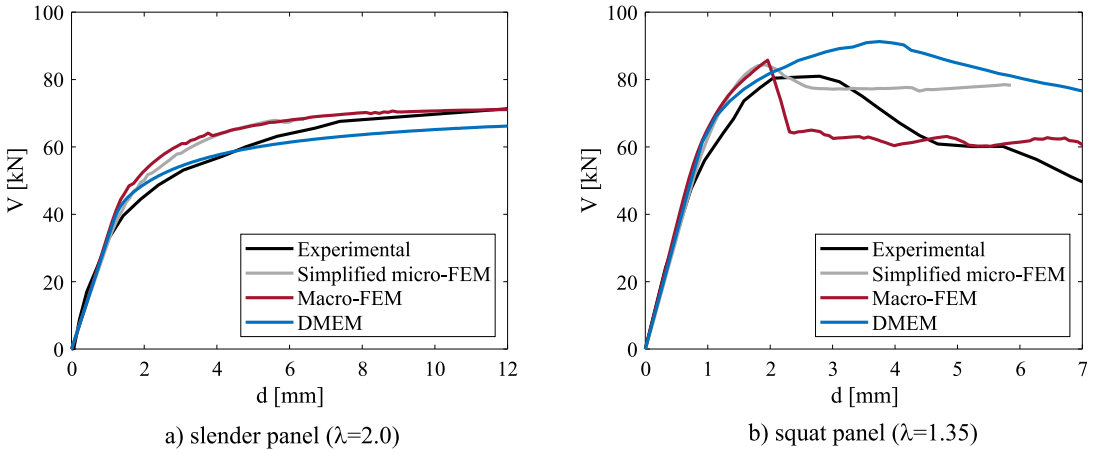

Fig. 3. Comparison between the experimental and numerical load–displacement curves. (For interpretation of the references to colour in this figure legend, the reader is referred to the web version of this article.)

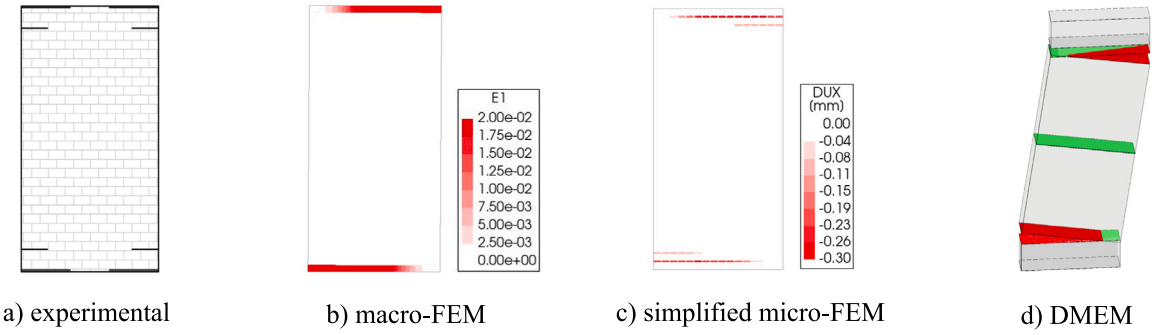

Fig. 4. Comparison of the experimental and numerical crack patterns in the slender masonry panel (peak capacity). (For interpretation of the references to colour in this figure legend, the reader is referred to the web version of this article.)

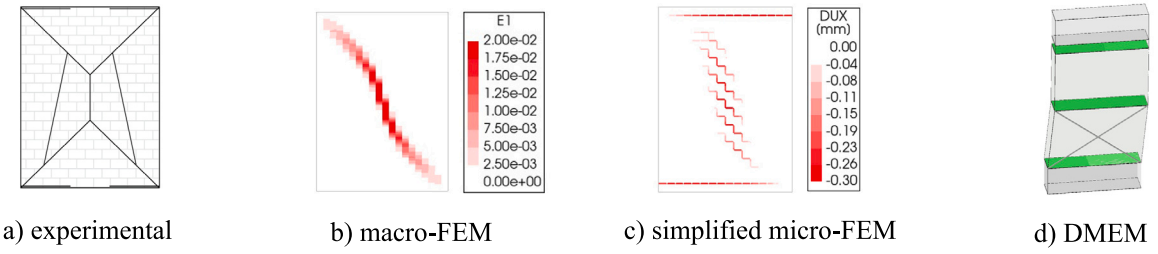

Fig. 5. Comparison of the experimental and numerical crack patterns in the squat masonry panel (peak capacity). (For interpretation of the references to colour in this figure legend, the reader is referred to the web version of this article.)

the latter case, the in-plane diagonal shear damage is represented with an 'x' at the centre of the macro-element. Results demonstrate that both macro- and micro-models predict a flexural failure for the slender wall, with the typical distribution of the cracks at the two end sections, and a shear diagonal failure for the squat wall with diagonal cracks extending from the corners towards the centre. Although the experimental refers to a cyclic analysis, it is noteworthy that a unidirectional analysis has been performed numerically. Therefore, considering the squat panel, an x-braced failure is clear in the experimental crack patterns of Fig. 5(a). Instead, Fig. 5(b)–(d) show only part of the latter failure since the load is unidirectional, thence the results are assumed to be representative and adequate for the numerical calibration.

4.2. Panel scale: sensitivity and partial safety factors

Prior to the calibration of the partial safety factors γ_m that account for the material uncertainty, sensitivity analyses are conducted to (i) identify the material parameters that mostly affect the output control parameter, which is herein assumed to be the ultimate load, and (ii) derive the corresponding sensitivity coefficients. Two quasi-static analyses are performed for each studied variable X_i: one in which the variable assumed a lower bound value defined to be the 5% percentile; and another for which the variable has an upper bound value defined to be its 95% percentile. The remaining random variables are given, for both cases, by the respective median value. Such a process is performed for all the studied parameters, with a total of nineteen variables considered for the simplified micro-FE models, five variables for the FE macro-models, and eight variables for the DME models (see Tables 1–3). The obtained sensitivity coefficients are reported in Fig. 6, in which the parameters associated with the mortar joint and the unit failure interface are represented as 'uj' and 'uu', respectively. Results evidence that when a macro-FE approach is adopted, the global behaviour of the panels is mainly dominated by the parameters related to the tensile regime (see Fig. 6a). However, in the case of the DME models, the

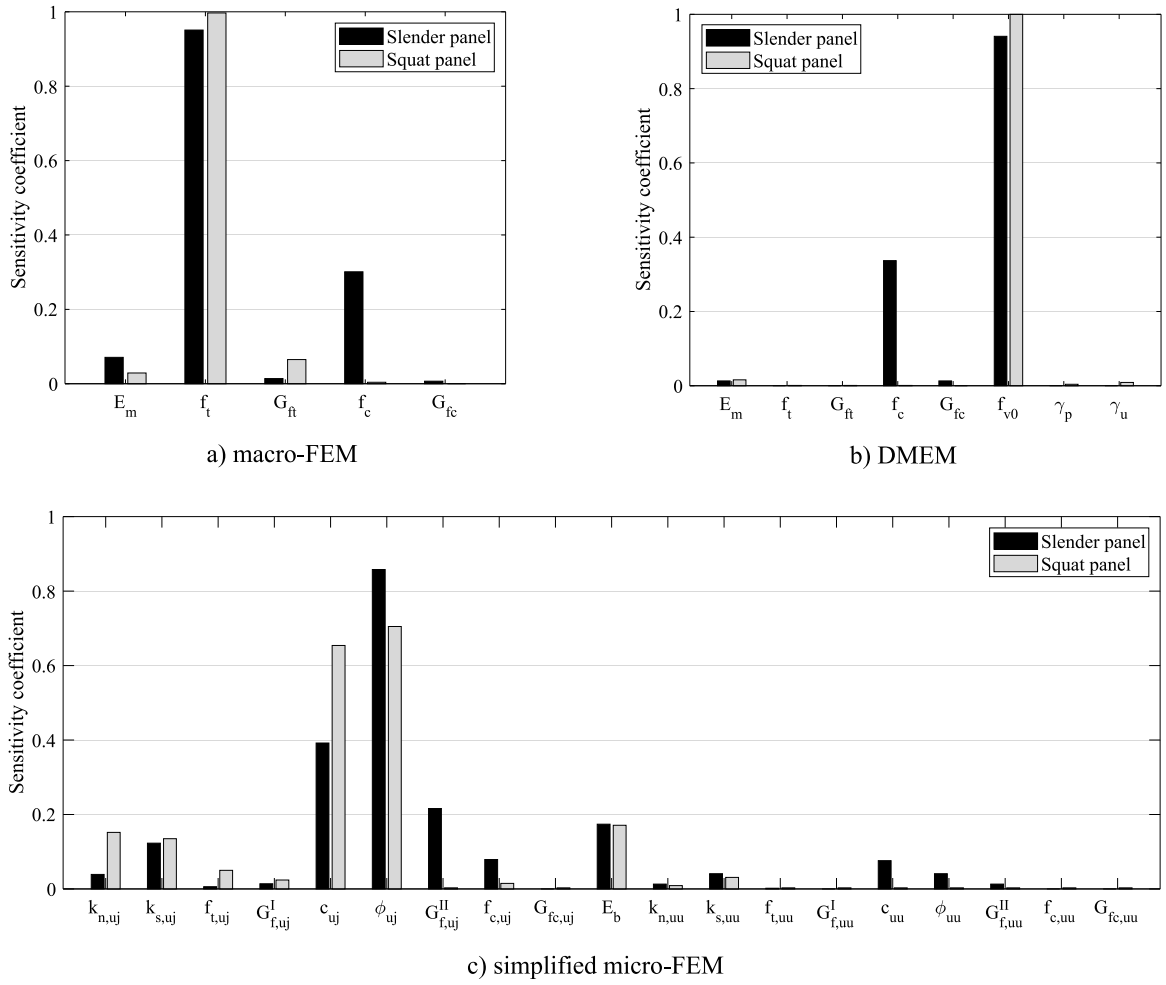

Fig. 6. Sensitivity coefficients for the random variables of the panel prototypes.

response is mainly influenced by the shear regime parameters (Fig. 6b). This difference is explained because the tensile and shear behaviours of masonry are modelled as uncoupled in the adopted discrete approach. As concerns the simplified micro-FE models (Fig. 6c), the global response of both panels is mainly influenced by the ones related to the tensile and shear regimes of the joint interface element. One can note that the parameters related to the brick units tend to have a lower influence on the global response. These findings are in agreement with experimental evidence concerning the case of weak mortar masonry, in which the tensile and shear regimes tend to govern the global structural behaviour [60].

The sensitivity coefficients reported in Fig. 6 are indicative of an axial load-ratio σ_0/f_c of 0.1. Given that the predominant failure mode is influenced by the applied axial load, its impact on the sensitivity coefficients was investigated for several σ_0/f_c values with reference to the DME model of the slender panel prototype. The results reported in Table 4 highlight that the α-values vary according to the applied axial load, in line with the shifts in the predominant failure mode.

Based on the results of the sensitivity analyses, the PSF accounting for material variability can be derived for the influential parameters, which are defined according to the threshold α-values (α_1) determined in Section 2. Table 5 presents the γ_m values for both slender and squat panels. These are reported for the influential parameters conditioned by each modelling strategy, probabilistic model (i.e. Normal (ND), Lognormal (LND), and Weibull (WD) distribution), and referring to a target reliability index of 2.5. The latter value corresponds to a CC2 (normal) and is adopted based on the evidence that most existing masonry buildings typically belong to the CC2 or CC3 (high) consequence classes

Table 4
Variation of the sensitivity factors with the axial load-ratio σ_0/f_c (the highest α-value for each σ_0/f_c value is reported in bold).

σ_0/f_c	Failure mode	E	f_t	G_{ft}	f_c	G_{fc}	f_{v0}	γ_p	γ_u
0.05	Flexural	0.04	0.00	0.00	**0.99**	0.03	0.00	0.00	0.00
0.1	Diagonal-shear	0.01	0.00	0.00	0.34	0.01	**0.94**	0.00	0.00
0.2	Diagonal-shear	0.00	0.00	0.00	0.00	0.00	**1.00**	0.00	0.00
0.4	Diagonal-shear	0.02	0.00	0.00	0.14	0.00	**0.99**	0.00	0.03
0.6	Crushing	0.04	0.00	0.00	**0.94**	0.04	0.37	0.00	0.00

of failure [32]. Thus, this choice ensures a more representative and applicable assessment for most of the existing masonry structures. For the micro-FE models, the parameters related to the potential brick crack interface are excluded from the calibration of the partial safety factors, as their influence on the global response was found to be negligible for a weak-mortar-strong-unit type [21]. By analysing Table 5, it is evident that the Weibull model tends to be more conservative, hence leading to higher partial factors. In contrast, the Lognormal model leads to less conservative values. This discrepancy is mainly due to a larger relative weighting of the left tail in the Weibull model and a lower one in the Lognormal model. Furthermore, the difference between models becomes more apparent for higher coefficients of variation, as shown in Fig. 7. The latter reports the variation of γ_m with reference to the Normal, Lognormal, and Weibull distributions and considering the highest (25.8%) and lowest (12.2%) CoV values among the adopted material parameters. Attention is thus required when selecting the probabilistic model for a resistance variable. In particular, the adoption of the Normal and Weibull models is recommended for variables with

Table 5
Partial safety factors accounting for the material variability in the panel prototypes.

Prototype	Modelling approach	Influential parameter	Probabilistic distribution		
			Normal	Lognormal	Weibull
Slender panel	Macro-FEM	f_t	1.28	1.16	1.36
	DMEM	f_{t0}	1.29	1.16	1.36
	Simplified micro-FEM	ϕ_{uj}	1.16	1.10	1.21
Squat panel	Macro-FEM	f_t	1.34	1.18	1.43
	DMEM	f_{t0}	1.38	1.19	1.47
	Simplified micro-FEM	ϕ_{uj}	1.03	1.02	1.04

Table 6
Partial safety factors that include material variability for the analysis of the wall prototype.

Prototype	Modelling approach	Influential parameter	Probabilistic distribution		
			Normal	Lognormal	Weibull
'Door Wall' façade	Macro-FEM	f_t	1.37	1.19	1.45
	DMEM	f_{t0}	1.38	1.19	1.46

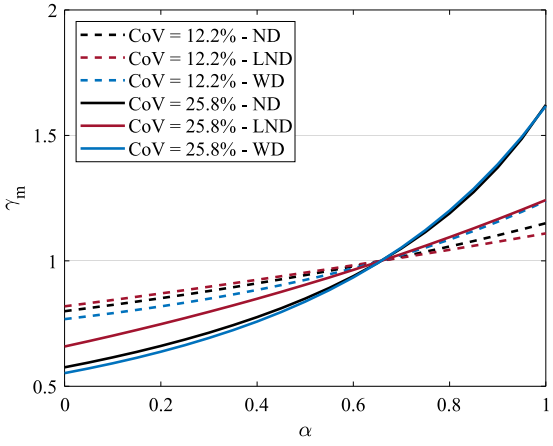

Fig. 7. Variation of the partial safety factor for material uncertainty γ_m considering different CoV values and probabilistic distributions. (For interpretation of the references to colour in this figure legend, the reader is referred to the web version of this article.)

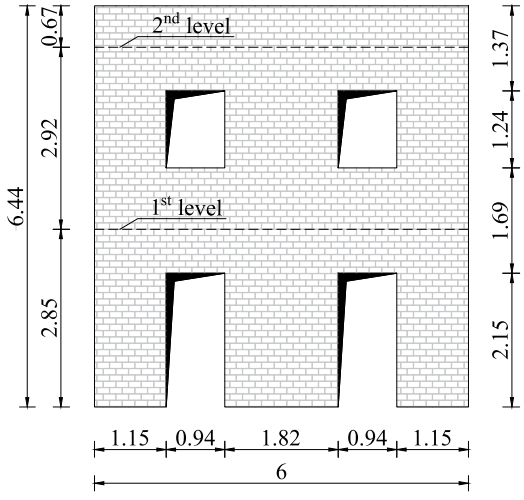

Fig. 8. Geometry of the 'Door wall' prototype (dimensions in m).

low CoV values, given that their degree of conservatism increases with the coefficient of variation, while the Lognormal model emerges as a more generally suitable alternative.

4.3. Wall scale: sensitivity and partial safety factors

The geometry of the wall assumed as a benchmark is given in Fig. 8 and was retrieved from a façade of the prototype known in literature as the "Door wall", which is part of a two-storey URM building tested by Calvi and Magenes [61,62]. This wall is selected since it is made with the same characteristics as the masonry components studied at a panel scale, thus guaranteeing the objectivity of the numerical calibration performed in Section 4.1. The wall presents a thickness of 0.25 m and is characterised by a regular opening arrangement, with two doors on the ground floor and two windows on the upper floor. The influence of transverse walls is neglected and the masonry façade is considered as restrained only at the base. The presence of reinforced concrete tie beams is assumed at each floor level and vertical loads equal to 20.7 and 19.7 kN/m are applied to the lower and upper floors, respectively, which align with rigid diaphragms. The wall is modelled according to the DMEM and macro-FEM approach by assuming the material properties reported in Table 1.

Sensitivity analyses are conducted following the procedure adopted in Section 4.2 aiming at the identification of the most relevant material parameters to the structural response of the URM wall prototype. The sensitivity coefficients reported in Fig. 9 highlight that the response is mainly influenced by the shear strength and the tensile strength for the DME and macro-FE model, respectively, which is consistent with the outcomes retrieved at a panel scale. Partial safety factors that account for the shear strength variability are derived considering the Normal, Lognormal, and Weibull distribution and with reference to a target reliability index of 2.5 (see Table 6). The computed values for γ_m are similar to the ones found at the panel scale (Section 4.2) since the global behaviour of the URM wall is mainly influenced by the failure of the ground floor piers, which have an aspect-ratio that is comparable with the masonry panel prototypes. The difference lies in the higher axial load-ratio of $\sigma_0/f_c = 0.20$ for the piers, in contrast to the $\sigma_0/f_c = 0.10$ ratio applied to the panel prototypes. Such consistency in the γ_m values can be clarified by observing that the influential parameters and their corresponding sensitivity coefficients tend to remain constant in the range of σ_0/f_c where a specific failure mode is prevailing, as demonstrated in Table 4.

5. Model uncertainty

The estimation of model uncertainty (θ_R) related to the prediction of the structural capacity of masonry structures is addressed. Such estimation is aligned with the methodologies presented in ISO 2394 [42] and EN 1990:2023 [32], for which θ_R is treated as a random variable that follows a lognormal distribution. The effect of geometric variability and testing errors is disregarded since it is assumed that the workmanship under the controlled laboratory conditions is of high quality. Workmanship defects in the specimen preparation are thus excluded, e.g. variation of mortar thickness, incorrect proportioning in mixing of the mortar, disturbance of bricks after laying on the mortar, and misalignment of wall panels. Consequently, θ_R reflects mainly

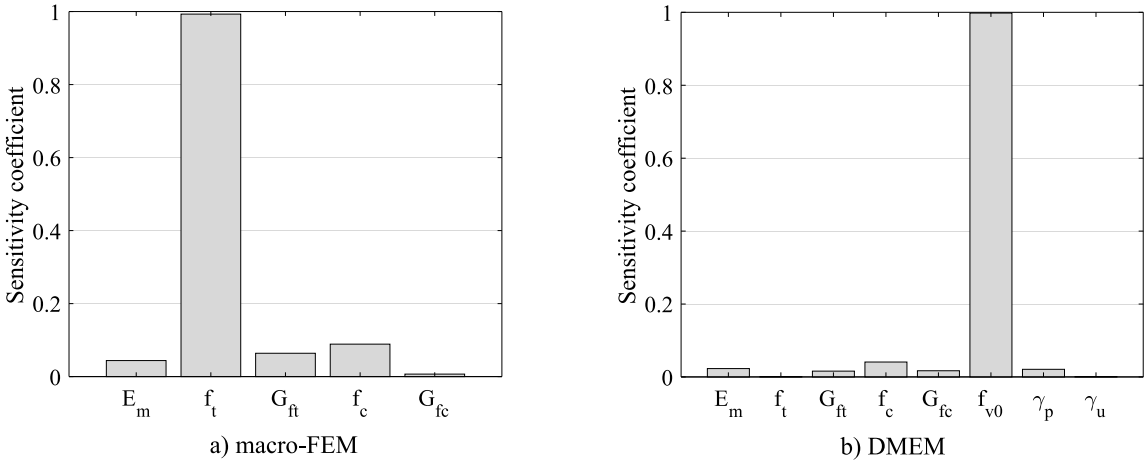

Fig. 9. Sensitivity coefficients of the 'Door wall' prototype.

Table 7
Statistical descriptors of model uncertainty θ_R.

Statistical descriptors of θ_R		Flexural failure (F)	Diagonal shear failure (DS)
Mean value	μ_θ	1.047	0.994
	m_θ	0.042	−0.008
Standard deviation	σ_θ	0.085	0.064
	s_θ	0.083	0.064
Coefficient of variation	CoV_θ	8.1%	6.4%

the deviation of the numerical results caused by numerical modelling simplifications and by the intrinsic phenomenological and formulation-based characteristics of each numerical strategy. In this regard, and to better understand the statistical properties of θ_R within shear–compression tests on URM panels, a literature review was conducted. The data gathered are presented in Appendix and refer only to regular masonry panel prototypes constrained in a double-fixed condition and subjected to a constant vertical overload and in-plane horizontal load. Such a dataset is compiled considering the correspondence between the experimental [57,63–66] and numerical [14,55,67–83] failure modes (F, flexure or DS, diagonal shear).

To better characterise the database, the values for the model uncertainty are also provided in Fig. 10a and Fig. 10b by discriminating the panel aspect-ratio ($\lambda = H/B$) and the axial load-ratio (σ_0/f_c). The evaluated panels have an aspect-ratio that ranges from 0.7 to 2.5 and an axial load-ratio of 0.03−0.20. Fig. 11a shows that the predicted shear capacity (V_{num}) is in general in good agreement with the experimental results (V_{exp}). The obtained mean values for θ_R (i.e. μ_θ) are close to 1.0 and show a low coefficient of variation (CoV_θ), as presented in Table 7. The suitability of a lognormal distribution for θ_R is verified by analysing the quantile–quantile plot between the normal probability of the logarithm of θ_R, which is reported in Fig. 10b. The close alignment of the data confirms that θ_R can be accurately represented with a lognormal distribution.

Based on the statistical descriptors of θ_R and from Eq. (7), a value of γ_{Rd} equal to 1.02 and 1.06 is derived for flexural and shear diagonal failure, respectively. The target reliability index is assumed to be equal to $\beta = 2.5$ in consistency with Section 4, while a value of $\alpha_\theta = 0.32$ is adopted for the FORM sensitivity factor for the model uncertainty, which corresponds to the recommended value by EN 1990:2023 [32] and ISO 2394 [42] for non-dominating resistance variables.

6. Probabilistic vs confidence factor approach: capacity assessment of masonry structures

An insight is provided into the consequences that different uncertainty propagation strategies have on the structural capacity assessment of masonry structures. The case studies analysed in Sections 4.2 and 4.3 are considered and three approaches are evaluated, namely: (i) the application of code-recommended confidence factors (CFs); (ii) the adoption of material PSF γ_M computed through the proposed procedure; and (iii) the use of a full-probabilistic approach based on the SDCP method. The CF-based assessment is conducted according to the recently updated EN 1998-3 [25] and the Italian Structural Code [26]. Concerning the former, the CFs (identified as γ_{Rd} in the updated version of EN 1998-3 [25]) are applied to the ultimate shear strength, which is derived by assuming the average values of the material properties. Since the adopted mechanical properties of masonry are based on experimental tests [57], the recommended values corresponding to KLM3 are employed, selecting 1.65 for flexural failure and 1.40 for diagonal shear failure [25]. In the case of the Italian Structural Code [26], the shear capacity is computed by dividing the average values of the strength parameters by a CF of 1.0, which corresponds to the KL3, and a γ_M value of 2.5, as recommended for masonry made with elements of category II and class I. To what concern the assessment based on the use of material PSF γ_M, the in-plane capacity is estimated according to Eq. (2). In particular, the average values of the strength parameters are divided by the PSF defined as $\gamma_M = \gamma_m \gamma_{Rd}$ based on the values of γ_m and γ_{Rd} calibrated in Sections 4 and 5, respectively. The γ_M values are reported in Table 8, for each analysed case study and adopted modelling strategy. In the case of the 'Door wall' prototype, γ_M is derived by assuming a value of γ_{Rd} equal to 1.06, which corresponds to the one calibrated for diagonal shear failure of URM panels in Section 5. This choice is motivated by the evidence that the global behaviour of the URM wall is mainly influenced by the response of the ground floor piers, which tend to exhibit a diagonal shear failure.

Since the latter strategy is based on a semi-probabilistic approach, a comparison with a full-probabilistic one is provided. In this case, the in-plane capacity is estimated based on the formulation presented in Eq. (1), where (i) the effect of material variability, accounted in $R\{\dots\}$, is evaluated through the SDCP method; and (ii) the model uncertainty is accounted through γ_{Rd}, with assumed values in line with those derived in Section 5. Concerning the former, two quasi-static analyses are performed for each N variable: one in which the variable

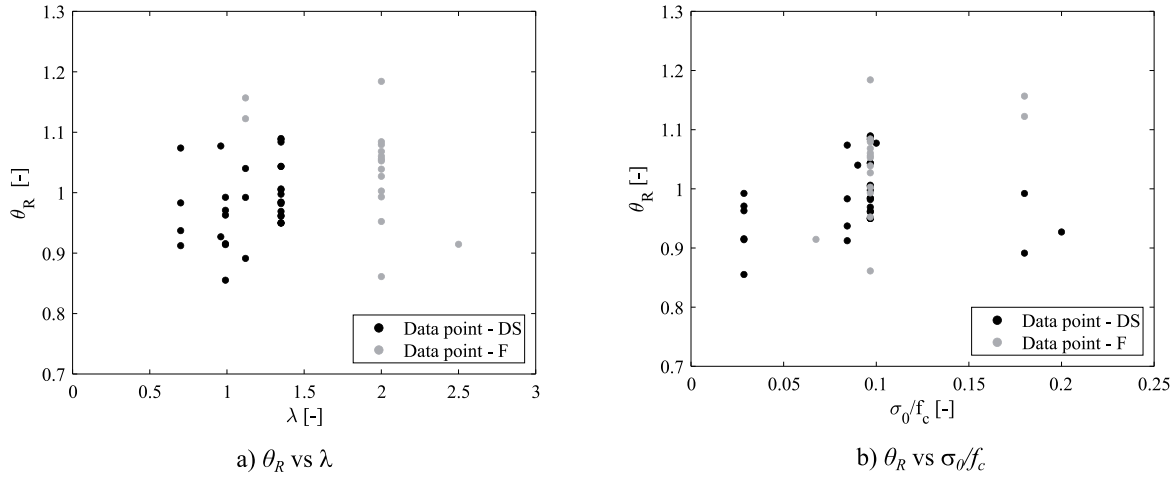

Fig. 10. Scatter of θ_R for panels with a diagonal shear (DS) or flexural (F) failure mode.

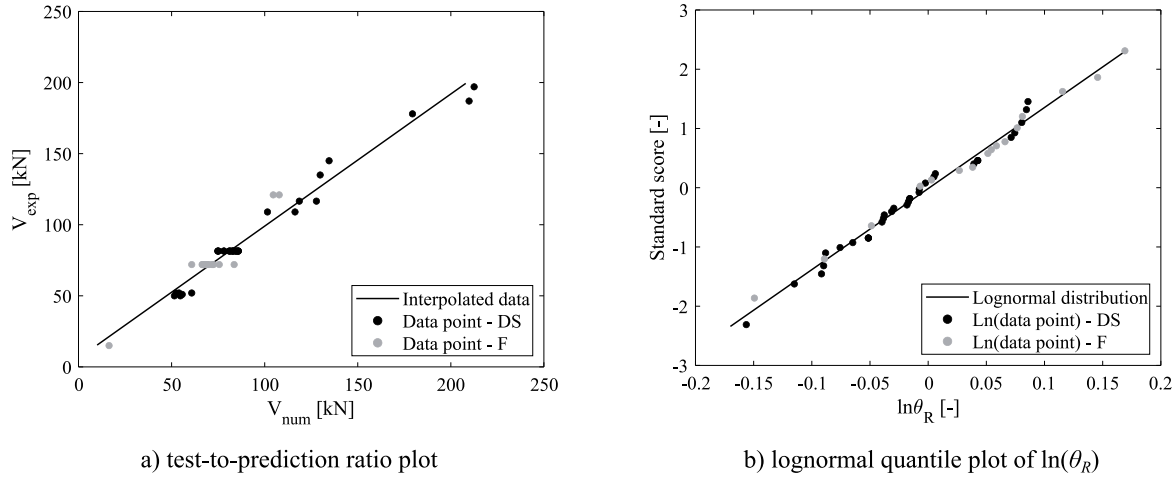

Fig. 11. Experimental and predicted shear capacity plot and (b) normal probability paper plot of the logarithm of θ_R.

Table 8
Partial safety factors (PSF) for material strength parameters that include material and model uncertainties.

Prototype	Modelling approach	Influential parameter	Probabilistic distribution		
			Normal	Lognormal	Weibull
Slender panel	Macro-FEM	f_t	1.32	1.18	1.39
	DMEM	f_{t0}	1.30	1.18	1.38
	Simplified micro-FEM	ϕ_{uj}	1.18	1.12	1.23
Squat panel	Macro-FEM	f_t	1.46	1.27	1.56
	DMEM	f_{t0}	1.42	1.25	1.52
	Simplified micro-FEM	ϕ_{uj}	1.10	1.08	1.11
'Door Wall' facade	Macro-FEM	f_t	1.47	1.26	1.57
	DMEM	f_{t0}	1.45	1.26	1.54

assumes a lower bound value defined to be the 5% percentile; and another, where the variable assumes an upper bound value defined to be the 95% percentile. The remaining random variables are given, for both cases, by the respective median values. An additional analysis is performed by adopting the average values for all uncertain parameters. Finally, $R\{\ldots\}$ is defined as the median value of the ultimate load resulting from the $2N+1$ quasi-static analyses. The comparison of the shear capacity estimation according to the three adopted approaches is reported in Fig. 12. The results obtained through the adoption of the proposed procedure (denoted in Fig. 12 as 'PSF') are presented considering the assumption of different probabilistic distributions to model material uncertainty, i.e. Normal (ND), Lognormal (LND), and Weibull (WD). As a reference, the ultimate load estimated by adopting the average material properties is reported (depicted in Fig. 12 as 'Exp. Cab.'). The shear capacity predictions based on the calibrated safety factors exhibit small variations based on the assumed model distribution. In particular, the differences are more pronounced in the case of the squat panel prototype. This result is strictly related to the value of the sensitivity coefficient of the influential parameter, which is higher in the case of the squat panel. As illustrated in Fig. 7, a high sensitivity coefficient implies that even a minor adjustment can result in significant changes in the partial safety factors, especially when the coefficient of variation (CoV) is also high. Furthermore, the adoption of the calibrated γ_M values leads to estimations that are, in most cases, on the safe side compared to the full-probabilistic analysis. On the other hand, the analyses performed according to the CF-based approaches

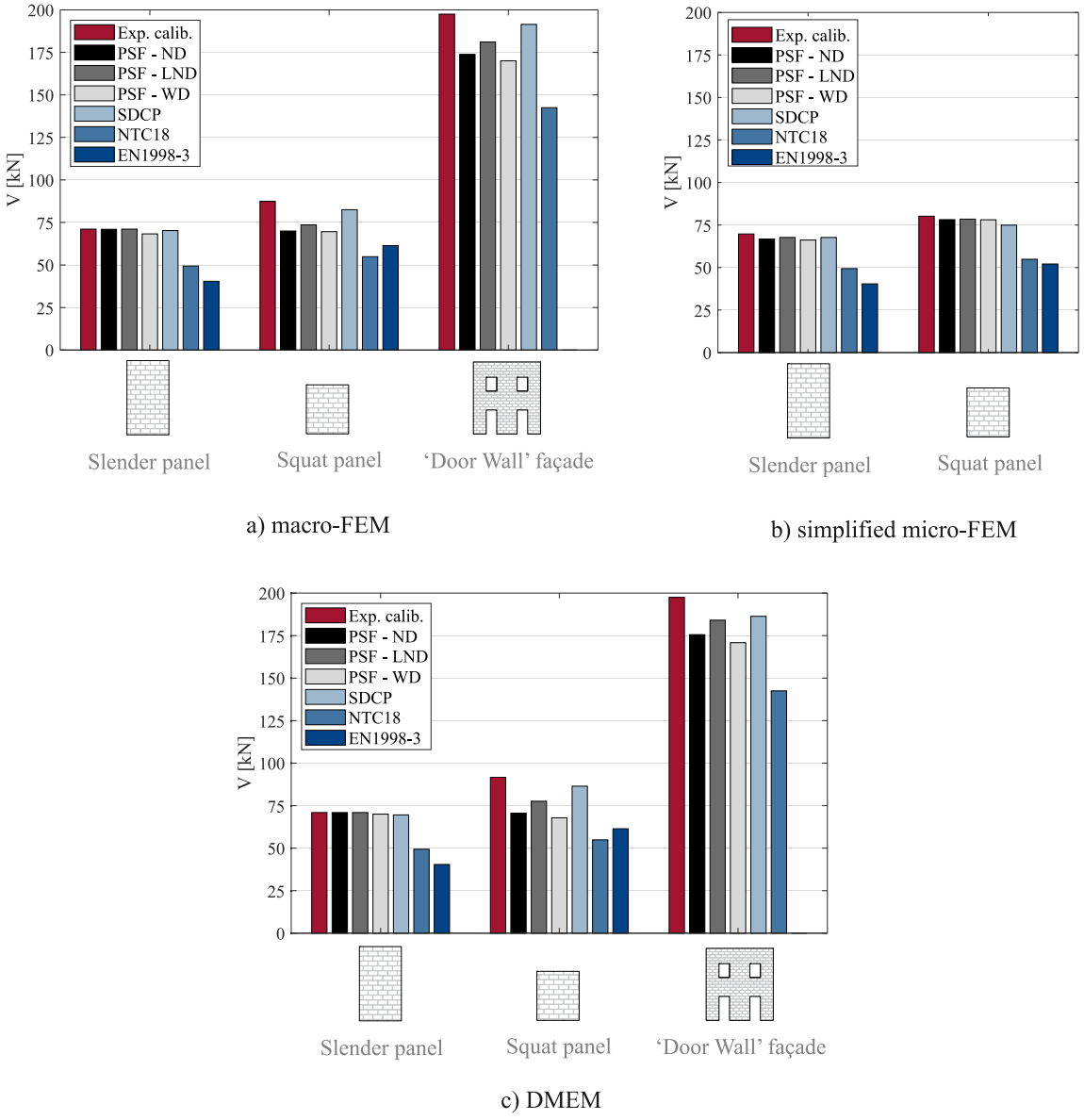

Fig. 12. Comparison of the shear capacity obtained through a probabilistic-based and a CF-based method. (For interpretation of the references to colour in this figure legend, the reader is referred to the web version of this article.)

tend to provide overly conservative estimates, especially for slender panels, exhibiting differences ranging up to 40% when compared to the other approaches. This outcome underscores a significant limitation of a CF-based approach, namely the adoption of predefined CF values that are only connected to the KL and unrelated to the structure under analysis. Indeed, despite ensuring a conservative result, adopting this approach may lead to the decision of not needed and costly retrofitting interventions. Therefore, the use of calibrated partial safety factors tailored to the specific characteristics of the structure provides a more rational assessment.

It is noteworthy that the estimation of θ_R may be affected by the probable calibration of the material parameters adopted in the considered research works. Indeed, it has been demonstrated that the lack of a full knowledge of the tested structures can lead to significant differences between numerical strategies [84,85]. A further exercise has been conducted to evaluate the effect of a lower accuracy of the numerical models on the shear capacity estimation. In this context, the material PSF have been calibrated with reference to the slender panel prototype modelled according to the DMEM approach. The γ_m value has been adopted consistently with the one calibrated in 4.2 with reference to the Weibull model, i.e. $\gamma_m = 1.36$, as it demonstrated its higher degree of conservativeness when compared to the other models. As regard to γ_{Rd}, a calibration test has been conducted by considering a standard deviation of θ_R equal to 0.166, which is double the value retrieved from the database. Despite the increased standard deviation, only a slight variation in the predicted shear capacity (i.e. 65.2 kN) has been reported compared to its initial value (i.e. 68.3 kN). This result is mainly due to the assumption of a non-dominating resistance variable for θ_R, corresponding to a sensitivity factor $\alpha_\theta = 0.32$ as recommended by EN 1990:2023 [32] and ISO 2394 [42]. Consequently, a calibration test has been conducted by increasing the sensitivity factor α_θ to 0.80, as recommended by the aforementioned standards for dominating resistance variables. This resulted in a predicted shear capacity of 57.4 kN, which is still higher than the results obtained through the CF-based approaches according to the recently updated EN 1998-3 [25] and the Italian Structural Code [26], which are 49.4 kN and 40.4 kN, respectively. These findings demonstrate the tendency of the CF-based approaches to provide conservative estimates.

7. Final remarks

A practice-oriented procedure for the calibration of material partial safety factors was presented. With the aim of reducing the computation time and complexity of a full-probabilistic approach, a FORM-based calibration was adopted to propagate both material and model uncertainties. First, the use of sensitivity analyses coupled with a SDCP method was explored to derive the corresponding partial safety factors for material uncertainty (γ_m). Several case studies with different geometries and either at a panel or façade wall scale were considered. The effect of different failure modes was evaluated, as well as the use of different numerical approaches (macro- and micro-modelling) within the framework of nonlinear static analyses. Second, the partial safety factors for model uncertainties (γ_{Rd}) were derived according to the methodologies outlined in ISO 2394 [42] and EN 1990:2023 [32]. To this end, the statistical properties of the numerical results related to the in-plane response of URM panels have been collected through a literature review. Here, it has been hypothesised as a good approach to recommend values for γ_{Rd} according to the predominant failure mode, i.e. a flexural and a shear diagonal failure.

The study addressed the effect of propagating uncertainties according to different strategies for the assessment of the structural capacity of masonry structures. Three approaches with different complexity levels were considered: (i) a full-probabilistic approach based on the SDCP method; (ii) the CF-based approach according to the recently updated EN 1998-3 [25] and the Italian Structural Code [26]; (iii) the adoption of partial safety factors for material property γ_M, defined as $\gamma_M = \gamma_m\gamma_{Rd}$, based on calibrated values of γ_m and γ_{Rd}.

The novelties of the study are threefold: (i) introduction of sensitivity analysis combined with the SDCP method to compute PSF for material uncertainty; (ii) investigation of the effects on PSF calibration when considering different geometries, failure modes, modelling strategies (i.e., discrete approach and FE-based continuum approach), and scales of analysis (i.e., panel and façade wall scales); (iii) derivation of statistical parameters from a literature dataset of numerical predictions for shear–compression tests to represent model uncertainties in estimating PSF.

The following points summarise the main findings and contributions of the paper:

- the key input parameters influencing the in-plane behaviour of masonry structures may vary based on the adopted modelling strategy. Their influence may also change when different levels of compressive loads are applied. However, it has been demonstrated that the relative importance of such parameters is kept consistent for a range of applied axial loads depending on the specific dominant failure mode (shear sliding, flexural, diagonal shear, and crushing). These ranges of axial load can be found through analytical criteria available in the literature [58,86] as well as in standards and guidelines [25,26]. In this study, the influencing parameters were evaluated for different compression levels within different failure domains, which may be impractical within a seismic assessment of a masonry structure. In such cases, it is suggested to evaluate the critical parameters according to a range of interest that is conditioned by the existing pre-compression level of the structure according to a self-weight analysis, as in Cattari et al. [87].
- the adoption of different probabilistic models for a resistance variable affects the calibration of PSF, particularly for variables with high CoV values. Specifically, the adoption of the Normal and Weibull models is recommended for variables with low CoV values as their degree of conservatism increases with the coefficient of variation. The Lognormal model seems more adequate in general;
- the results from a quantile–quantile plot of θ_R confirm the suitability of a lognormal distribution for model uncertainties, in line with the recommendations outlined in ISO 2394 [42] and EN 1990:2023 [32];
- the adoption of standard-based values for the CF can lead to overly conservative estimates. This underscores a primary limitation of the CF-based approach, which lies in the application of pre-determined CF values independently of the type of structural system;
- the comparison of the in-plane capacity prediction based on the use of a full-probabilistic approach and on the adoption of calibrated γ_M values proved the suitability of the proposed procedure in replacing a full probabilistic analysis without compromising the uncertainty representativeness, while guaranteeing results on the safe side.

Finally, further investigations are necessary to better understand the potential of the proposed approach in capturing the propagation of material and model uncertainties in the case of out-of-plane behaviour in masonry structures. Additional efforts are also required to include the effect of the geometrical variability in the computation of γ_M.

Funding

This work was partly financed by FCT/MCTES, Portugal through national funds (PIDDAC) under the R&D Unit Institute for Sustainability and Innovation in Structural Engineering (ISISE), under reference UIDB/04029/2020 (doi.org/10.54499/UIDB/04029/2020), and under the Associate Laboratory Advanced Production and Intelligent Systems ARISE under reference LA/P/0112/2020. This work was partly funded by national funds through FCT – Foundation for Science and Technology, Portugal, under grant agreement 2022.12559.BD attributed to the 1st author. This work was partly supported by project STAND4HERITAGE that has received funding from the European Research Council (ERC) under the European Union's Horizon 2020 research and innovation programme (Grant agreement No. 833123), as an Advanced Grant.

CRediT authorship contribution statement

Federica Vadalà: Writing – review & editing, Writing – original draft, Visualization, Validation, Software, Methodology, Data curation, Conceptualization. **Luis C.M. da Silva:** Writing – review & editing, Supervision, Methodology, Conceptualization. **Ivo Caliò:** Writing – review & editing, Supervision, Software. **Paulo B. Lourenço:** Writing – review & editing, Supervision.

Declaration of competing interest

The authors declare the following financial interests/personal relationships which may be considered as potential competing interests: Federica Vadaà reports financial support was provided by Foundation for Science and Technology. Federica Vadalà reports financial support was provided by European Research Council. Paulo B. Lourenço reports financial support was provided by European Research Council. If there are other authors, they declare that they have no known competing financial interests or personal relationships that could have appeared to influence the work reported in this paper

Data availability

Data will be made available on request.

Appendix. Database of model uncertainty observation

See Table A.1.

Table A.1
Database of model uncertainty observation.

Authors	Modelling approach	Representation scale	Reference experimental test	σ_0/f_c	λ	Failure mode	V_{num}	V_{exp}	$\theta_{Rd} = V_{exp}/V_{num}$
Bomben et al., 2023 [83]	EFM	Macro-scale	Anthoine et al., 1994 [57]	0.10	2.00	F	68.2	72.0	1.06
	EFM	Macro-scale	Anthoine et al., 1994 [57]	0.10	2.00	F	67.4	72.0	1.07
	EFM	Macro-scale	Anthoine et al., 1994 [57]	0.10	2.00	F	66.4	72.0	1.08
	EFM	Macro-scale	Anthoine et al., 1994 [57]	0.10	1.35	DS	75.2	81.5	1.08
	EFM	Macro-scale	Anthoine et al., 1994 [57]	0.10	1.35	DS	74.9	81.5	1.09
	EFM	Macro-scale	Anthoine et al., 1994 [57]	0.10	1.35	DS	74.8	81.5	1.09
Calderini and Lagomarsino, 2008 [67]	FEM	Macro-scale	Anthoine et al., 1994 [57]	0.10	2.00	F	71.8	72.0	1.00
	FEM	Macro-scale	Anthoine et al., 1994 [57]	0.10	1.35	DS	78.1	81.5	1.04
Caliò et al., 2012 [55]	DMEM	Macro-scale	Anthoine et al., 1994 [57]	0.10	2.00	F	60.8	72.0	1.18
	DMEM	Macro-scale	Anthoine et al., 1994 [57]	0.10	1.35	DS	81.1	81.5	1.00
Casolo and Peña, 2007 [14]	DEM	Macro-scale	Anthoine et al., 1994 [57]	0.10	2.00	F	83.6	72.0	0.86
	DEM	Macro-scale	Anthoine et al., 1994 [57]	0.10	1.35	DS	84.1	81.5	0.97
Dolatshahi et al., 2018 [74]	FEM	Micro-scale	Petry and Beyer, 2015 [64]	0.18	1.12	DS	209.8	187.0	0.89
	FEM	Micro-scale	Petry and Beyer, 2015 [64]	0.18	1.12	DS	179.4	178.0	0.99
	FEM	Micro-scale	Petry and Beyer, 2015 [64]	0.09	1.12	DS	129.8	135.0	1.04
	FEM	Micro-scale	Petry and Beyer, 2015 [64]	0.18	1.12	F	107.8	121.0	1.12
Gatta et al., 2018 [75]	FEM	Macro-scale	Anthoine et al., 1994 [57]	0.10	2.00	F	68.4	72.0	1.05
	FEM	Macro-scale	Anthoine et al., 1994 [57]	0.10	1.35	DS	82.8	81.5	0.98
Kesavan and Menon, 2022 [80]	FEM	Micro-scale	Anthoine et al., 1994 [57]	0.10	1.35	DS	82.8	81.5	0.98
Minga et al., 2018 [76]	FEM	Macro-scale	Anthoine et al., 1994 [57]	0.10	2.00	F	70.1	72.0	1.03
	FEM	Macro-scale	Anthoine et al., 1994 [57]	0.10	1.35	DS	83.0	81.5	0.98
Morandini at al., 2022 [81]	AEM	Micro-scale	Anthoine et al., 1994 [57]	0.10	2.00	F	69.3	72.0	1.04
	EFM	Macro-scale	Anthoine et al., 1994 [57]	0.10	2.00	F	66.7	72.0	1.08
	AEM	Micro-scale	Anthoine et al., 1994 [57]	0.10	1.35	DS	84.7	81.5	0.96
	EFM	Macro-scale	Anthoine et al., 1994 [57]	0.10	1.35	DS	81.7	81.5	1.00
Penna et al., 2014 [69]	EFM	Macro-scale	Anthoine et al., 1994 [57]	0.10	2.00	F	67.9	72.0	1.06
	EFM	Macro-scale	Anthoine et al., 1994 [57]	0.10	1.35	DS	85.8	81.5	0.95
Petracca et al., 2016 [71]	FEM	Macro-scale	Raijmakers and Vermeltfoort, 1992 [63]	0.03	0.99	DS	54.0	52.0	0.96
	FEM	Micro-scale	Raijmakers and Vermeltfoort, 1992 [63]	0.03	0.99	DS	52.4	52.0	0.99
Pulatsu et al., 2020 [78]	DEM	Micro-scale	Raijmakers and Vermeltfoort, 1992 [63]	0.03	0.99	DS	54.7	52.0	0.95

(*continued on next page*)

Table A.1 (*continued*).

Authors	Modelling approach	Representation scale	Reference experimental test	σ_0/f_c	λ	Failure mode	V_{num}	V_{exp}	$\theta_{Rd} = V_{exp}/V_{num}$
Raka et al., 2015 [70]	EFM	Macro-scale	Anthoine et al., 1994 [57]	0.10	2.00	F	63.2	72.0	1.14
	EFM	Macro-scale	Anthoine et al., 1994 [57]	0.10	1.35	DS	72.1	81.5	1.13
Rinaldin et al., 2016 [72]	EFM	Macro-scale	Anthoine et al., 1994 [57]	0.10	2.00	F	72.5	72.0	0.99
	EFM	Macro-scale	Anthoine et al., 1994 [57]	0.10	1.35	DS	81.0	81.5	1.01
Saloustros et al., 2018 [77]	FEM	Macro-scale	Anthoine et al., 1994 [57]	0.10	1.35	DS	84.8	81.5	0.96
Sousamli et al., 2022 [82]	FEM	Macro-scale	Anthoine et al., 1994 [57]	0.10	2.00	F	75.6	72.0	0.95
	FEM	Macro-scale	Anthoine et al., 1994 [57]	0.10	1.35	DS	78.1	81.5	1.04
	FEM	Macro-scale	Messali et al., 2020 [66]	0.08	0.70	DS	118.6	116.6	0.98
	FEM	Macro-scale	Messali et al., 2020 [66]	0.08	0.70	DS	101.5	109.0	1.07
Wilding et al., 2017 [73]	FEM	Micro-scale	Salmanpour et al., 2015 [65]	0.20	0.96	DS	212.5	197.0	0.93
	FEM	Micro-scale	Salmanpour et al., 2015 [65]	0.10	0.96	DS	134.6	145.0	1.08
	FEM	Micro-scale	Petry and Beyer, 2015 [64]	0.18	1.12	F	104.6	121.0	1.16
Xie et al., 2021 [79]	FEM	Micro-scale	Messali et al., 2020 [66]	0.08	0.70	DS	127.8	116.6	0.91
	FEM	Micro-scale	Messali et al., 2020 [66]	0.07	2.5	F	16.4	15.0	0.91
	FEM	Micro-scale	Messali et al., 2020 [66]	0.08	0.70	DS	116.3	109.0	0.94
	FEM	Micro-scale	Raijmakers and Vermeltfoort, 1992 [63]	0.03	0.99	DS	51.5	52.0	1.01
Zucchini and Lourenço, 2009 [68]	FEM	Macro-scale	Raijmakers and Vermeltfoort, 1992 [63]	0.03	0.99	DS	60.8	52.0	0.86
	FEM	Micro-scale	Raijmakers and Vermeltfoort, 1992 [63]	0.03	0.99	DS	55.7	52.0	0.93

Modelling approaches: AEM = Applied Element Method; DEM= Discrete Element Method; DMEM = Discrete Macro-Element Method; EFM = Equivalent Frame Method; FEM = Finite Element Method.
Failure modes: DS = Diagonal Shear; F = Flexural.

References

[1] Silva LC, Lourenço PB, Milani G. Derivation of the out-of-plane behaviour of masonry through homogenization strategies: Micro-scale level. Comput Struct 2018;209:30–43. http://dx.doi.org/10.1016/j.compstruc.2018.08.013.

[2] Nodargi NA, Bisegna P. A mixed finite element for the nonlinear analysis of in-plane loaded masonry walls. Internat J Numer Methods Engrg 2019;120(11):1227–48. http://dx.doi.org/10.1002/NME.6179.

[3] Funari MF, Hajjat AE, Masciotta MG, Oliveira DV, Lourenço PB. A parametric scan-to-FEM framework for the digital twin generation of historic masonry structures. Sustainability 2021;13(19). http://dx.doi.org/10.3390/SU131911088.

[4] Lo Monaco A, Grillanda N, Onescu I, Fofiu M, Clementi F, D'Amato M, et al. Seismic assessment of Romanian Orthodox masonry churches in the Banat area through a multi-level analysis framework. Eng Fail Anal 2023;153. http://dx.doi.org/10.1016/J.ENGFAILANAL.2023.107539.

[5] Schiavoni M, Giordano E, Roscini F, Clementi F. Advanced numerical insights for an effective seismic assessment of historical masonry aggregates. Eng Struct 2023;285. http://dx.doi.org/10.1016/J.ENGSTRUCT.2023.115997.

[6] Bui TT, Limam A, Sarhosis V, Hjiaj M. Discrete element modelling of the in-plane and out-of-plane behaviour of dry-joint masonry wall constructions. Eng Struct 2017;136:277–94. http://dx.doi.org/10.1016/j.engstruct.2017.01.020.

[7] Kim J, Lorenzoni F, Salvalaggio M, Valluzzi MR. Seismic vulnerability assessment of free-standing massive masonry columns by the 3D Discrete Element Method. Eng Struct 2021;246. http://dx.doi.org/10.1016/j.engstruct.2021.113004.

[8] Chen S, Ferrante A, Clementi F, Bagi K. DEM analysis of the effect of bond pattern on the load bearing capacity of barrel vaults under vertical loads. Int J Masonry Res Innov 2021;6(3):346–73. http://dx.doi.org/10.1504/IJMRI.2021.116234.

[9] Schiavoni M, Giordano E, Roscini F, Clementi F. Numerical modeling of a majestic masonry structure: A comparison of advanced techniques. Eng Fail Anal 2023;149. http://dx.doi.org/10.1016/J.ENGFAILANAL.2023.107293.

[10] Ferrante A, Schiavoni M, Bianconi F, Milani G, Clementi F. Influence of stereotomy on discrete approaches applied to an ancient church in Muccia, Italy. J Eng Mech 2021;147(11). http://dx.doi.org/10.1061/(ASCE)EM.1943-7889.0002000.

[11] Chácara C, Cannizzaro F, Pantò B, Caliò I, Lourenço PB. Assessment of the dynamic response of unreinforced masonry structures using a macroelement modeling approach. Earthq Eng Struct Dyn 2018;47(12):2426–46. http://dx.doi.org/10.1002/EQE.3091.

[12] Cannizzaro F, Pantò B, Caddemi S, Caliò I. A Discrete Macro-Element Method (DMEM) for the nonlinear structural assessment of masonry arches. Eng Struct 2018;168:243–56. http://dx.doi.org/10.1016/J.ENGSTRUCT.2018.04.006.

[13] Vadalà F, Cusmano V, Funari MF, Caliò I, Lourenço PB. On the use of a mesoscale masonry pattern representation in discrete macro-element approach. J Build Eng 2022;50. http://dx.doi.org/10.1016/J.JOBE.2022.104182.

[14] Casolo S, Peña F. Rigid element model for in-plane dynamics of masonry walls considering hysteretic behaviour and damage. Earthq Eng Struct Dyn 2007;36(8):1029–48. http://dx.doi.org/10.1002/EQE.670.

[15] Casolo S. Macroscale modelling of microstructure damage evolution by a rigid body and spring model. J Mech Mater Struct 2009;4(3):551–70. http://dx.doi.org/10.2140/JOMMS.2009.4.551.

[16] Silva LC, Lourenço PB, Milani G. Nonlinear discrete homogenized model for out-of-plane loaded masonry walls. J Struct Eng 2017;143(9). http://dx.doi.org/10.1061/(ASCE)ST.1943-541X.0001831.

[17] Maria D'altri A, Sarhosis V, Milani G, Rots J, Cattari S, Lagomarsino S, et al. Modeling strategies for the computational analysis of unreinforced masonry structures: Review and classification. Arch Comput Methods Eng 2020;27:1153–85. http://dx.doi.org/10.1007/s11831-019-09351-x.

[18] Dolsek M. Incremental dynamic analysis with consideration of modeling uncertainties. Earthq Eng Struct Dyn 2009;38(6):805–25. http://dx.doi.org/10.1002/EQE.869.

[19] Saloustros S, Pelà L, Contrafatto FR, Roca P, Petromichelakis I. Analytical derivation of seismic fragility curves for historical masonry structures based on stochastic analysis of uncertain material parameters. Int J Archit Heritage 2019;13(7):1142–64. http://dx.doi.org/10.1080/15583058.2019.1638992.

[20] Tomić I, Vanin F, Beyer K. Uncertainties in the seismic assessment of historical masonry buildings. Appl Sci 2021;11(5). http://dx.doi.org/10.3390/APP11052280.

[21] da Silva LC, Milani G, Lourenço PB. Probabilistic-based discrete model for the seismic fragility assessment of masonry structures. Structures 2023;52:506–23. http://dx.doi.org/10.1016/J.ISTRUC.2023.04.015.

[22] Federal Emergency Management Agency (FEMA). Pre-standard and commentary for the seismic rehabilitation of buildings, FEMA 356. Tech. rep., 2000.

[23] Cornell CA, Jalayer F, Hamburger RO, Foutch DA. The probabilistic basis for the 2000 SAC/FEMA steel moment frame guidelines. J Struct Eng 2002;128(4):526–33. http://dx.doi.org/10.1061/(ASCE)0733-9445(2002)128:4(526).

[24] CNR-DT 212/2013. Guide for the Probabilistic Assessment of the Seismic Safety of Existing Buildings. Tech. rep., 2014.

[25] CEN/TC250. Eurocode 8: Design of structures for earthquake resistance – Part 3: Assessment and retrofitting of buildings (EN 1998-3). Tech. rep., European Committee of Standardization. Technical Committee 250; 2005.

[26] Ministero delle Infrastrutture e dei Trasporti (MIT). Circolare 21 gennaio 2019, Istruzioni per l'applicazione dell'Aggiornamento delle "Norme tecniche per le costruzioni" di cui al decreto ministeriale 17/1/2018 (in italian). Tech. rep., 2019.

[27] Tondelli M, Rota M, Penna A, Magenes G. Evaluation of uncertainties in the seismic assessment of existing masonry buildings. J Earthq Eng 2012;16(SUPPL. 1):36–64. http://dx.doi.org/10.1080/13632469.2012.670578.

[28] Rota M, Penna A, Magenes G. A framework for the seismic assessment of existing masonry buildings accounting for different sources of uncertainty. Earthq Eng Struct Dyn 2014;43:1045–66. http://dx.doi.org/10.1002/eqe.2386.

[29] Cattari S, Karatzetzou A, Degli Abbati S, Pitilakis D, Negulescu C, Gkoktsi K. Seismic performance based assessment of the arsenal de milly of the Medieval city of rhodes. Comput Methods Appl Sci 2015;37:365–92. http://dx.doi.org/10.1007/978-3-319-16130-3_15.

[30] Franchin P, Pagnoni T. A general model of resistance partial factors for seismic assessment and retrofit. In: 16th European conference on earthquake engineering. 2018, p. 1–12.

[31] Haddad J, Cattari S, Lagomarsino S. Use of the model parameter sensitivity analysis for the probabilistic-based seismic assessment of existing buildings. Bull Earthq Eng 2019;17(4):1983–2009. http://dx.doi.org/10.1007/s10518-018-0520-8.

[32] CEN/TC250. Eurocode - Basis of structural and geotechnical design (EN 1990:2023). Tech. rep., European Committee of Standardization. Technical Committee 250; 2023.

[33] Hasofer AM, Lind NC. Exact and invariant second-moment code format. J Eng Mech Div 1974;100(1):111–21. http://dx.doi.org/10.1061/JMCEA3.0001848.

[34] Jacinto L, Santos LO, Neves LC. Calibration of partial safety factors using FORM. Revista Portuguesa de Engenharia de Estruturas 2020;Ed. LNEC.(14):29–42.

[35] Caspeele R, Sykora M, Allaix DL, Steenbergen R. The design value method and Adjusted Partial Factor Approach for existing structures. Struct Eng Int: J Int Assoc Bridge Struct Eng (IABSE) 2013;23(4):386–93. http://dx.doi.org/10.2749/101686613X13627347100194.

[36] Mojsilović N, Stewart MG. Probability and structural reliability assessment of mortar joint thickness in load-bearing masonry walls. Struct Saf 2015;52(PB):209–18. http://dx.doi.org/10.1016/J.STRUSAFE.2014.02.005.

[37] Li G, Lu Z, Li L, Ren B. Aleatory and epistemic uncertainties analysis based on non-probabilistic reliability and its kriging solution. Appl Math Model 2016;40(9–10):5703–16. http://dx.doi.org/10.1016/J.APM.2016.01.017.

[38] Jafari S. Material characterisation of existing masonry: a strategy to determine strength, stiffness and toughness properties for structural analysis (Ph.D. thesis), Delft University of Technology; 2021, http://dx.doi.org/10.4233/uuid:3bcbbc72-0212-44e9-ac86-2fdc54ec5987.

[39] Müller D. Probabilistic assessment of existing masonry structures – the influence of spatially variable material properties and a Bayesian method for determining structure-specific partial factors (Ph.D. thesis), Technische Universität Darmstadt; 2022, http://dx.doi.org/10.26083/tuprints-00022997.

[40] Joint Commitee on Structural Safety (JCSS). Probabilistic model code - part 3: Resistance models. Tech. rep., 2011.

[41] Holický M, Retief JV, Sýkora M. Assessment of model uncertainties for structural resistance. Probab Eng Mech 2016;45:188–97. http://dx.doi.org/10.1016/J.PROBENGMECH.2015.09.008.

[42] International Organization for Standardization (ISO/TC98/SC22015). General principles on reliability for structures (ISO 2394). Tech. rep., 2015.

[43] König G, Hosser D. The simplified level II method and its application on the derivation of safety elements for level I. Tech. rep., Paris: CEB Bulletin d'Information No. 147, 02/1982, Comité Euro-international du Béton; 1982.

[44] Sobol I. Sensitivity estimates for nonlinear mathematical models. Math Model Comput Exp 1993;4:404–14.

[45] Papaioannou I, Straub D. Variance-based reliability sensitivity analysis and the FORM α-factors. Reliab Eng Syst Saf 2021;210. http://dx.doi.org/10.1016/j.ress.2021.107496.

[46] Sykora M, Diamantidis D, Holicky M, Jung K. Target reliability for existing structures considering economic and societal aspects. Struct Infrastruct Eng 2017;13(1):181–94. http://dx.doi.org/10.1080/15732479.2016.1198394.

[47] Vrouwenvelder T, Scholten N. Assessment criteria for existing structures. Struct Eng Int 2018;20(1):62–5. http://dx.doi.org/10.2749/101686610791555595.

[48] NEN 8700:2011. Assessment of existing structures in case of reconstruction and disapproval - Basic rules (in dutch). Tech. rep., Nederlands Normalisatie Instituut; 2011.

[49] DIANA FEA BV. DIANA - DIsplacement method ANALizer. Tech. rep., 2024.

[50] Gruppo Sismica srl. HiStrA - Computer program for modelling historical and monumental masonry buildings. Tech. rep., 2024.

[51] Vecchio FJ, Collins MP. The modified compression-field theory for reinforced concrete elements subjected to shear. ACI J 1986;83(2):219–31. http://dx.doi.org/10.14359/10416.

[52] Parisse F, Marques R, Cattari S, Lourenço PB. Finite Element and Equivalent Frame modeling approaches for URM buildings: Implications of different assumptions in the seismic assessment. J Build Eng 2022;61. http://dx.doi.org/10.1016/J.JOBE.2022.105230.

[53] Lourenço PB, Rots JG. Multisurface interface model for analysis of masonry structures. J Eng Mech 1997;123(7):660–8. http://dx.doi.org/10.1061/(asce)0733-9399(1997)123:7(660).

[54] Van Zijl G. Computational modelling of masonry creep and shrinkage (Ph.D. thesis), Delft University of Technology; 2000.

[55] Caliò I, Cannizzaro F, Pantò B. A macro-element approach for modeling the nonlinear behaviour of monumental buildings under static and seismic loadings. In: World conference in earthquake engineering. 2012.

[56] Turnšek V, Čačovič F. Some experimental results on the strength of brick masonry walls. In: Proceedings of the 2nd international brick masonry conference. 1971, p. 149–56.

[57] Anthoine A, Magonette G, Magenes G. Shear-compression testing and analysis of brick masonry walls. In: Proceedings of the 10th European conference on earthquake engineering. 1994.

[58] Magenes G, Calvi GM. In-plane seismic response of brick masonry walls. Earthq Eng Struct Dyn 1997;26:1091–112. http://dx.doi.org/10.1002/(SICI)1096-9845(199711)26:11.

[59] D'Altri AM, Cannizzaro F, Petracca M, Talledo DA. Nonlinear modelling of the seismic response of masonry structures: Calibration strategies. Bull Earthq Eng 2022;20(4):1999–2043. http://dx.doi.org/10.1007/S10518-021-01104-1.

[60] Willis C, Griffith M, Lawrence S. Horizontal bending of unreinforced clay brick masonry walls. Masonry Int 2004;17:109–21.

[61] Calvi GM, Magenes G. Experimental research on response of URM building systems. In: Proceedings of the U.S. Italy workshop on guidelines for seismic evaluation and rehabilitation of unreinforced mansory buildings. 1994.

[62] Magenes G, Kingsley G, Calvi GM. Seismic testing of a full-scale, two-story masonry building: Test procedure and measured experimental response. Tech. rep., 1995.

[63] Raijmakers TMJ, Vermeltfoort AT. Deformation Controlled Tests in Masonry Shear Walls (Report B-92-1156) (in dutch). Tech. rep., Delft, The Netherlands; 1992.

[64] Petry S, Beyer K. Cyclic test data of six unreinforced masonry walls with different boundary conditions. Earthq Spectra 2015;31(4):2459–84. http://dx.doi.org/10.1193/101513EQS269/ASSET/IMAGES/LARGE/10.1193_101513EQS269-FIG19.JPEG.

[65] Salmanpour AH, Mojsilović N, Schwartz J. Displacement capacity of contemporary unreinforced masonry walls: An experimental study. Eng Struct 2015;89:1–16. http://dx.doi.org/10.1016/J.ENGSTRUCT.2015.01.052.

[66] Messali F, Esposito R, Ravenshorst GJ, Rots JG. Experimental investigation of the in-plane cyclic behaviour of calcium silicate brick masonry walls. Bull Earthq Eng 2020;18(8):3963–94. http://dx.doi.org/10.1007/S10518-020-00835-X/TABLES/10.

[67] Calderini C, Lagomarsino S. Continuum model for in-plane anisotropic inelastic behavior of masonry. J Struct Eng 2008;134(2):209–20. http://dx.doi.org/10.1061/(ASCE)0733-9445(2008)134:2(209).

[68] Zucchini A, Lourenço PB. A micro-mechanical homogenisation model for masonry: Application to shear walls. Int J Solids Struct 2009;46(3–4):871–86. http://dx.doi.org/10.1016/J.IJSOLSTR.2008.09.034.

[69] Penna A, Lagomarsino S, Galasco A. A nonlinear macroelement model for the seismic analysis of masonry buildings. Earthq Eng Struct Dyn 2014;43(2):159–79. http://dx.doi.org/10.1002/EQE.2335.

[70] Raka E, Spacone E, Sepe V, Camata G. Advanced frame element for seismic analysis of masonry structures: model formulation and validation. Earthq Eng Struct Dyn 2015;44(14):2489–506. http://dx.doi.org/10.1002/EQE.2594.

[71] Petracca M, Pelà L, Rossi R, Oller S, Camata G, Spacone E. Regularization of first order computational homogenization for multiscale analysis of masonry structures. Comput Mech 2016;57(2):257–76. http://dx.doi.org/10.1007/S00466-015-1230-6/TABLES/7.

[72] Rinaldin G, Amadio C, Macorini L. A macro-model with nonlinear springs for seismic analysis of URM buildings. Earthq Eng Struct Dyn 2016;45(14):2261–81. http://dx.doi.org/10.1002/EQE.2759.

[73] Wilding BV, Dolatshahi KM, Beyer K. Influence of load history on the force-displacement response of in-plane loaded unreinforced masonry walls. Eng Struct 2017;152:671–82. http://dx.doi.org/10.1016/J.ENGSTRUCT.2017.09.038.

[74] Dolatshahi KM, Nikoukalam MT, Beyer K. Numerical study on factors that influence the in-plane drift capacity of unreinforced masonry walls. Earthq Eng Struct Dyn 2018;47(6):1440–59. http://dx.doi.org/10.1002/EQE.3024.

[75] Gatta C, Addessi D, Vestroni F. Static and dynamic nonlinear response of masonry walls. Int J Solids Struct 2018;155:291–303. http://dx.doi.org/10.1016/J.IJSOLSTR.2018.07.028.

[76] Minga E, Macorini L, Izzuddin BA. A 3D mesoscale damage-plasticity approach for masonry structures under cyclic loading. Meccanica 2018;53(7):1591–611. http://dx.doi.org/10.1007/S11012-017-0793-Z/FIGURES/25.

[77] Saloustros S, Cervera M, Pelà L. Tracking multi-directional intersecting cracks in numerical modelling of masonry shear walls under cyclic loading. Meccanica 2018;53(7):1757–76. http://dx.doi.org/10.1007/S11012-017-0712-3/FIGURES/14.

[78] Pulatsu B, Gonen S, Erdogmus E, Lourenço PB, Lemos JV, Hazzard J. Tensile fracture mechanism of masonry wallettes parallel to bed joints: A stochastic discontinuum analysis. Modelling 2020;1(2):78–93. http://dx.doi.org/10.3390/MODELLING1020006.

[79] Xie Z, Sousamli M, Messali F, Rots JG. A sub-stepping iterative constitutive model for cyclic cracking-crushing-shearing in masonry interface elements. Comput Struct 2021;257. http://dx.doi.org/10.1016/J.COMPSTRUC.2021.106654.

[80] Kesavan P, Menon A. Investigation of in-plane and out-of-plane interaction in unreinforced masonry piers by block-based micro-modeling. Structures 2022;46:1327–44. http://dx.doi.org/10.1016/J.ISTRUC.2022.10.105.

[81] Morandini C, Malomo D, Penna A. Equivalent frame discretisation for URM façades with irregular opening layouts. Bull Earthq Eng 2022;20(5):2589–618. http://dx.doi.org/10.1007/S10518-022-01315-0/TABLES/5.

[82] Sousamli M, Messali F, Rots JG. A total-strain based orthotropic continuum model for the cyclic nonlinear behavior of unreinforced brick masonry structures. Internat J Numer Methods Engrg 2022;123(8):1813–40. http://dx.doi.org/10.1002/NME.6917.

[83] Bomben L, Rinaldin G, Fasan M, Amadio C. Survey on non-linear cyclic responses of Unreinforced Masonry buildings by means of commercial finite-element codes. Proc Struct Integrity 2023;44:434–41. http://dx.doi.org/10.1016/J.PROSTR.2023.01.057.

[84] Tomić I, Penna A, DeJong M, Butenweg C, Correia AA, Candeias PX, et al. Shake-table testing of a stone masonry building aggregate: overview of blind prediction study. Bull Earthq Eng 2023. http://dx.doi.org/10.1007/S10518-022-01582-X/TABLES/18.

[85] Parisse F, Cattari S, Marques R, Lourenço PB, Magenes G, Beyer K, et al. Benchmarking the seismic assessment of unreinforced masonry buildings from a blind prediction test. Structures 2021;31:982–1005. http://dx.doi.org/10.1016/J.ISTRUC.2021.01.096.

[86] Mann W, Müller H. Failure of shear-stressed masonry: an enlarged theory, tests and application to shear walls. In: Proceedings of the british ceramic society. 1982.

[87] Cattari S, Camilletti D, D'Altri AM, Lagomarsino S. On the use of continuum Finite Element and Equivalent Frame models for the seismic assessment of masonry walls. J Build Eng 2021;43:102519. http://dx.doi.org/10.1016/J.JOBE.2021.102519.